

An investigation on the maximum earthquake input energy for elastic SDOF systems

Onur Merter*

Department of Civil Engineering, Usak University, 64100, Usak, Turkey

(Received December 7, 2018, Revised March 13, 2019, Accepted March 17, 2019)

Abstract. Energy-based seismic design of structures has gradually become prominent in today's structural engineering investigations because of being more rational and reliable when it is compared to traditional force-based and displacement-based methods. Energy-based approaches have widely taken place in many previous studies and investigations and undoubtedly, they are going to play more important role in future seismic design codes, too. This paper aims to compute the maximum earthquake energy input to elastic single-degree-of-freedom (SDOF) systems for selected real ground motion records. A data set containing 100 real ground motion records which have the same site soil profiles has been selected from Pacific Earthquake Research (PEER) database. Response time history (RTH) analyses have been conducted for elastic SDOF systems having a constant damping ratio and natural periods of 0.1 s to 3.0 s. Totally 3000 RTH analyses have been performed and the maximum mass normalized earthquake input energy values for all records have been computed. Previous researchers' approaches have been compared to the results of RTH analyses and an approach which considers the pseudo-spectral velocity with Arias Intensity has been proposed. Graphs of the maximum earthquake input energy versus the maximum pseudo-spectral velocity have been obtained. The results show that there is a good agreement between the maximum input energy demands of RTH analysis and the other approaches and the maximum earthquake input energy is a relatively stable response parameter to be used for further seismic design and evaluations.

Keywords: energy-based approach; ground motion record; the maximum earthquake input energy; response time history analysis; pseudo-spectral velocity

1. Introduction

In traditional earthquake-resistant design of structures the strength-based seismic design procedure is accepted and the strong ground motion effect is considered as equivalent static lateral forces which are obtained from the design acceleration response spectra. Analysis methods taking part in many previous and current seismic design codes (or documents) such as ATC-40 (1996), UBC (1997), Eurocode 8 (2004), FEMA-440 (2005), NBCC (2005), IBC (2006), TSDC (2007), ASCE/SEI 7-10 (2010) and TBEC (2018) generally take into consideration the strength and displacement capacity of structural members. These traditional procedures are based on the peak ground acceleration ignoring the effects of earthquake duration and hysteretic behavior. However, the energy parameter not only considers the effect of these parameters but also it can describe the structural behavior more rational under seismic effects (Uang and Bertero 1990, Fajfar and Fischinger 1990, Akbas and Shen 2003, Dindar *et al.* 2015). The energy-based seismic design methodology can handle the seismic problem more accurately than methodologies based on strength and displacement because it includes both strength and displacement characteristics of structures. The effect of

strong ground motions on structures has been interpreted in terms of energy by many researchers and the topic has gradually gained extensive attention in the field of earthquake engineering. The use of energy concept in seismic design was initially proposed by Housner (1956) and after then various researchers applied energy principles to earthquake-resistant structural design. Analytical and empirical many equations were proposed for determination of earthquake input energy because of being a primary step of energy-based earthquake engineering (Akiyama 1985, Kuwamura and Galambos 1989, Fajfar *et al.* 1989, Uang and Bertero 1990, Manfredi 2001, Benavent-Climent *et al.* 2002, Khashaee 2004, López-Almansa *et al.* 2013, Dindar *et al.* 2015). This primary step plays a crucial role in energy-based structural design since the energy dissipation in structural members by both elastic and inelastic behavior depends upon the knowledge of earthquake input energy. The input energy is a very stable quantity except in the short period range of structures and it is governed primarily by the natural period and the mass (López-Almansa *et al.* 2013). Therefore, the earthquake input energy spectra have become effective tools for determination of energy input to SDOF systems having a specific mass, natural period and damping ratio. The use of input energy spectra covers a wide range of ground motion and structural characteristics and they can be created for elastic and inelastic systems (Fajfar and Vidic 1994, Dindar *et al.* 2015). The maximum earthquake input energy of a SDOF system with a specific mass and damping ratio can be obtained by using the input

*Corresponding author, Assistant Professor
E-mail: onur.merter@usak.edu.tr

energy spectra graphs. In the input energy spectra, the maximum value of the input energy corresponds to a definite natural vibration period of the system. The input energy generally tends to decrease after this period value is exceeded. Zahrah and Hall (1984), Akiyama (1985) indicated that the maximum input energy per unit mass has a relatively stable parameter in the predominant period region of a ground motion and it is mainly influenced by characteristics of ground motion (Taflampas *et al.* 2008, López-Almansa *et al.* 2013).

There have been many fundamental studies in literature concerning the energy concept in earthquake-resistant and performance-based design of structures. Lee and Goel (2001), Leelataviwat *et al.* (2002) used the energy-balance, yield mechanism and target drift concepts to derive seismic design forces for multi-degree-of-freedom (MDOF) systems. Akbas (1997), Akbas *et al.* (2001, 2006, 2009) made detailed investigations and comprehensive evaluations for the energy concept in structural engineering, energy-based design methodology, hysteretic energy demand and energy response of moment-resisting frames. Liao (2010) investigated performance-based plastic design of reinforced concrete moment frames using energy-balance concept under seismic effects. Bojórquez *et al.* (2011) evaluated structural reliability of steel frames in terms of plastic hysteretic energy. A procedure which uses balances of the seismic energy demand and energy capacity of structures was proposed to calculate target displacements of reinforced concrete structures by Ucar *et al.* (2012). Enderami *et al.* (2014) proposed an energy-based approach to predict seismic demands of steel structures at the near-fault sites. Energy-based design base shear forces based on pre-selected failure mechanism and target story drift ratio were derived by Merter and Ucar (2017) for multistory RC frame structures. Gullu *et al.* (2018) discussed the seismic energy demands of multi-degree-of-freedom (MDOF) systems and they showed the distribution of hysteretic energy between structural elements and among the stories of structures.

Earthquake input energy spectra have been widely studied in literature for decades. Fajfar and Vidic (1994) presented a procedure for the determination of inelastic design spectra (for hysteretic and input energy). They proposed a simple formula to estimate the ratio of hysteretic energy to input energy (Fajfar and Vidic 1994). Decanini and Mollaioli (1998) formulated elastic earthquake input energy spectra of SDOF systems for different soil site classes. Mezgebo (2015) proposed input energy spectra for SDOF systems considering different hysteretic models and soil site classes. Dindar *et al.* (2015) made development of earthquake energy demand spectra for different soil classes. Mezgebo and Lui (2016) developed input and hysteretic energy spectra equations to be used in energy-based seismic design for different soil classes, hysteresis models and ductility levels. Gullu *et al.* (2017) showed experimentally validation of the input energy spectrum suggested by Dindar *et al.* (2015). Ozsarac *et al.* (2017) studied energy-based response of SDOF systems by using simulated ground motions. They conducted time history analyses and investigated earthquake input energy spectra for different soil site classes, damping ratios, source to site distances and earthquake magnitudes (Ozsarac *et al.* 2017).

The maximum earthquake input energy is a relatively stable response parameter to be used for further seismic design and therefore it is of importance to calculate it practically. In this study, 100 real ground motion data set has been selected from Pacific Earthquake Research (PEER) database to investigate the maximum input energy response of elastic SDOF systems. All of the selected near-fault and far-fault ground motions are on site class D according to National Earthquake Hazards Reduction Program (NEHRP; Building Seismic Safety Council [BSSC] 2009) site classification. The average shear-wave velocities in the top thirty meters of the soil (V_{S30}) have been selected between the value of 180 m/s and 360 m/s (For Site Class D: Stiff soil with $180 \text{ m/s} < V_{S30} \leq 360 \text{ m/s}$). SDOF systems have a constant damping ratio of 5% and natural vibration periods have been taken from 0.1 s to 3.0 s. Totally 3000 RTH analyses have been performed and the maximum mass normalized earthquake input energy values for all records have been computed. Maximum input energy values have been obtained from Housner's approximation (Housner 1956) and Khashae's expression (Khashae 2004) too. An approach which considers the pseudo-spectral velocity with Arias Intensity has been proposed within the study. The graphical relation of the maximum earthquake input energy with the maximum pseudo-spectral velocity has been investigated using the results of RTH analyses, previous researchers' expressions (Housner 1956, Khashae 2004) and the proposed approach. The results of analyses show that there is a good agreement between the maximum input energy demands of RTH analysis and the proposed approach, except ground motions having larger Arias intensities.

2. Energy equation and input energy

Energy-based structural design concept and energy related seismic design parameters are first formulated for SDOF systems. The seismic response of a lumped-mass SDOF system subjected to an earthquake excitation is governed by the following general equation of motion (Chopra 1995):

$$m \cdot \ddot{u} + c \cdot \dot{u} + f_s(u) = -m \cdot \ddot{u}_g(t) \quad (1)$$

where u is the relative displacement with respect to ground, m is the mass, \dot{u} is the velocity of the mass, \ddot{u} is the acceleration of the mass, c is the coefficient of viscous damping, $f_s(u)$ is the resisting force and $\ddot{u}_g(t)$ is the strong ground acceleration. Energy response parameters of a SDOF system may be expressed by integrating Eq. (1) over the relative displacement as

$$\int_0^{u(t)} m \cdot \ddot{u} \, du + \int_0^{u(t)} c \cdot \dot{u} \, du + \int_0^{u(t)} f_s(u) \, du = - \int_0^{u(t)} m \cdot \ddot{u}_g(t) \, du \quad (2)$$

Eq. (2) shows the energy balance equality for a SDOF system which is under the effect of earthquake ground motion. The equation can be turned into a time integral introducing $du = \dot{u} \, dt$ as (t is the entire duration of the earthquake)

$$\int_0^t m \cdot \ddot{u} \cdot \dot{u} \, dt + \int_0^t c \cdot \dot{u}^2 \, dt + \int_0^t f_s(u) \cdot \dot{u} \, dt = - \int_0^t m \cdot \ddot{u}_g(t) \cdot \dot{u} \, dt \quad (3)$$

Eq. (3) may be expressed in general type of energy components as below

$$E_K + E_\xi + E_S = E_I \quad (4)$$

where E_K is the kinetic energy, E_ξ is the damping energy, E_S is the total absorbed energy and E_I is the seismic input energy. The right-hand side of Eq. (4), which represents the input energy E_I , is the total of the energy components E_K , E_ξ and E_S . The total absorbed energy by the structure is composed of two parts as elastic strain energy E_{Se} , and hysteretic energy E_H which is the main energy component in nonlinear behavior. So Eq. (4) may be rewritten as

$$E_K + E_\xi + [E_{Se} + E_H] = E_I \quad (5)$$

The kinetic energy E_K and the elastic energy E_{Se} come to zero after the earthquake motion. These energies do not contribute to the structural damage. However, the most significant contribution to the structural damage comes from the hysteretic energy E_H . The hysteretic energy is referred as the most important energy component in scientific researches and it is mostly associated to the seismic structural damage (Fajfar and Vidic 1994, Manfredi 2001, Riddell and Garcia 2001, Mezgebo and Lui 2016).

The hysteretic energy E_H will be zero, if the structure remains linear elastic. In this case, the input energy will only be equal to the sum of the kinetic, damping and elastic strain energies (Eq. (5)). Energy time history graph of a linear elastic SDOF system having natural vibration period of $T=0.8$ sec and viscous damping ratio of $\xi=5\%$ is shown in Fig. 1. The energy time history graph is illustrated for 1940 Imperial Valley-02 earthquake ground motion (El Centro Array#9 Station)). It can be seen from the figure that the instant kinetic energy E_K and the elastic strain energy E_{Se} consist of relatively small portion of the input energy at any time during the vibration and it vanishes at the end of the ground motion.

3. Earthquake ground motion records

A total of 100 recorded actual accelerograms having strike-slip focal mechanism are selected to investigate the maximum

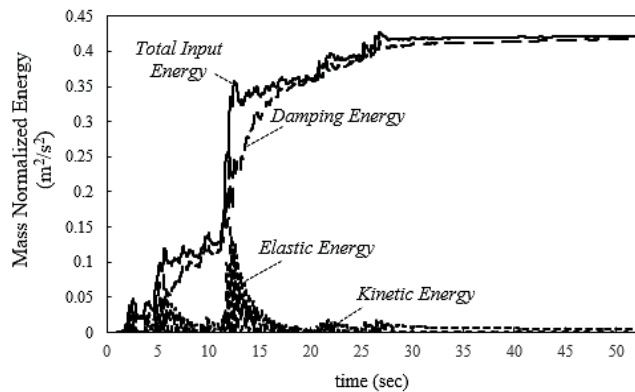


Fig. 1 Energy time history graph of a linear elastic SDOF system having $T=0.8$ sec and $\xi=5\%$ (for ground motion of the 1940 Imperial Valley-02 (El Centro Array#9 Station))

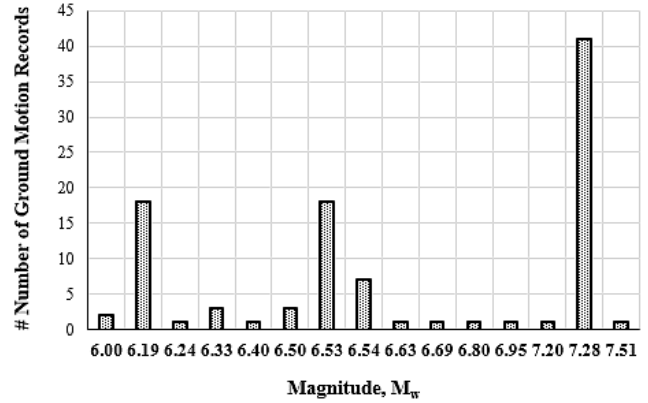


Fig. 2 Number of selected ground motions corresponding to moment magnitudes (M_w)

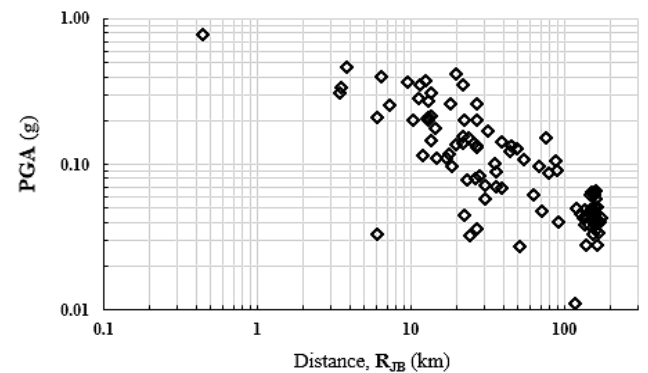


Fig. 3 Distribution of ground motion data for distance R_{JB} in terms of PGA (g)

earthquake input energies of linear elastic SDOF systems. The average shear-wave velocities in the top thirty meters of the soil (V_{S30}) are between the value of 180 m/s and 360 m/s. Soil site class is D (stiff soil with $180 \text{ m/s} < V_{S30} \leq 360 \text{ m/s}$) according to National Earthquake Hazards Reduction Program site classification (NEHRP; Building Seismic Safety Council 2009). Moment magnitudes (M_w) of selected earthquakes are between 6.0 and 7.51 and Joyner-Boore distances (R_{JB}) are between 0 km and 175 km. Moment magnitudes (M_w) of selected earthquakes are graphically shown in Fig. 2.

The peak ground accelerations (PGA) are between the values of 0.011 g and 0.777 g. All of the selected accelerograms in the study are obtained from the database of Pacific Earthquake Engineering Research Center, PEER (2018). Characteristics of selected accelerograms are shown in Table 1, Table 2 and Table 3, respectively (as part I, II and III). I_A is the Arias Intensity, as defined by Arias (1970), and it is proportional to the square of the ground acceleration integrated over time. PGA , PGV and PGD are the peak ground acceleration, peak ground velocity and peak ground displacement. Distribution of ground motion data for distance R_{JB} in terms of PGA is given in Fig. 3.

Ground motion records between the number of 1 and 34 are presented in Table 1, ground motions 35-67 are presented in Table 2 and ground motions 68-100 are presented in Table 3. Some records are used for more than one station and each record has different values of I_A , R_{JB} ,

Table 1 Selected earthquake ground motions (Set I: EQ 1-34) (PEER 2018)

Event Name (*1)	Station	Year	M_w	I_A (m/s)	R_{JB} (km)	V_{S30} (m/s)	PGA (g)	PGV (cm/s)	PGD (cm)
Big Bear	San B. - E & Hospitality	1992	6.46	0.3	34.98	296.97	0.101	11.90	3.35
Borrego Mtn	El Centro Array 9#	1968	6.63	0.2	45.12	213.44	0.133	26.70	14.60
Erzincan	Erzincan	1992	6.69	1.8	0	352.05	0.496	78.10	28.01
Kocaeli	Duzce	1999	7.51	1.3	13.6	281.86	0.312	58.80	44.11
Landers	Yermo Fire	1992	7.3	0.71	23.62	353.6	0.152	29.70	24.69
Nicaragua-01	Managua ESSO	1972	6.24	2	3.51	288.77	0.337	30.70	6.16
Trinidad	Rio Dell Overpass	1980	7.2	0.4	76.06	311.75	0.151	8.86	3.60
Imp. Valley-02	El Centro Array #9	1940	6.95	1.6	6.09	213.44	0.211	31.32	24.16
Northw. Calif-02	Ferndale City Hall	1941	6.6	0	91.15	219.31	0.040	6.83	4.48
Northern Calif-01	Ferndale City Hall	1941	6.4	0.1	44.52	219.31	0.122	13.53	5.30
Northern Calif-03	Ferndale City Hall	1954	6.5	0.5	26.72	219.31	0.203	52.40	39.40
El Alamo	El Centro Array #9	1956	6.8	0.1	121	213.44	0.050	14.16	16.34
Parkfield	Cholame – Sh. Array #5	1966	6.19	0.9	9.58	289.56	0.368	22.51	4.56
Parkfield	Cholame – Sh. Array #8	1966	6.19	0.4	12.9	256.82	0.272	11.36	3.81
Imp. Valley-06	Aeropuerto Mexicali	1979	6.53	1.2	0	259.86	0.271	24.19	3.71
Imp. Valley-06	Bonds Corner	1979	6.53	6.1	0.44	223.03	0.777	44.93	15.10
Imp. Valley-06	Calexico Fire Station	1979	6.53	0.9	10.45	231.23	0.203	18.65	15.88
Imp. Valley-06	Calipatria Fire Station	1979	6.53	0.1	23.17	205.78	0.078	27.36	27.41
Imp. Valley-06	Chihuahua	1979	6.53	1.2	7.29	242.05	0.254	29.89	7.65
Imp. Valley-06	Coachella Canal #4	1979	6.53	0.2	49.1	336.49	0.128	32.00	13.03
Imp. Valley-06	Compuertas	1979	6.53	0.4	13.52	259.86	0.147	9.32	2.89
Imp. Valley-06	Delta	1979	6.53	3.3	22.03	242.05	0.350	32.99	20.17
Imp. Valley-06	El Centro Array #1	1979	6.53	0.3	19.76	237.33	0.136	10.97	7.10
Imp. Valley-06	El Centro Array #11	1979	6.53	2	12.56	196.25	0.379	44.60	21.32
Imp. Valley-06	El Centro Array #12	1979	6.53	0.4	17.94	196.88	0.118	45.98	53.39
Imp. Valley-06	El Centro Array #13	1979	6.53	0.3	21.98	249.92	0.139	13.65	7.73
Imp. Valley-06	El Centro Array #8	1979	6.53	1.6	3.86	206.08	0.466	52.07	41.12
Imp. Valley-06	Niland Fire Station	1979	6.53	0.2	35.64	212	0.070	8.57	5.17
Imp. Valley-06	Parachute Test Site	1979	6.53	0.2	12.69	348.69	0.206	17.71	12.19
Imp. Valley-06	Plaster City	1979	6.53	0.1	30.33	316.64	0.058	5.85	2.49
Imp. Valley-06	Victoria	1979	6.53	0.3	31.92	242.05	0.168	8.84	1.93
Imp. Valley-06	Westmorland Fire Sta	1979	6.53	0.1	14.75	193.67	0.111	22.60	11.25
Victoria_Mexico	Chihuahua	1980	6.33	0.4	18.53	242.05	0.097	18.49	18.41
Victoria_Mexico	SAHOP Casa Flores	1980	6.33	0.1	39.1	259.59	0.069	8.94	2.18

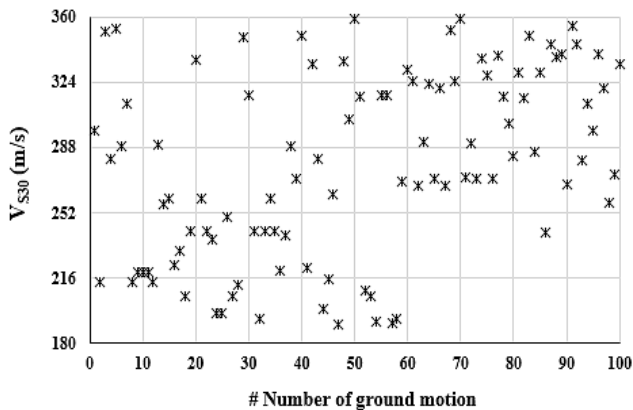


Fig. 4 The average shear-wave velocities (V_{S30}) in the top thirty meters of the soil for selected earthquakes

V_{S30} , PGA , PGV and PGD . The average shear-wave velocities (V_{S30}) in the top thirty meters of the soil for selected earthquakes within the study is graphically shown

in Fig. 4 ($180 \text{ m/s} < V_{S30} \leq 360 \text{ m/s}$).

4. Time history analyses and input energy results

Dynamic time history analyses are performed for linear elastic SDOF systems using the software PRISM (2011). Viscous damping ratio is considered as $\xi:5\%$. Newmark time integration method is used by the software. An illustrative figure for linear elastic SDOF system is shown in Fig. 5. Natural vibration periods of SDOF systems are taken from T_n : 0.1 s to 3.0 s (with a 0.1 s period step) and linear time history analyses are performed for each period values. 30-time history analyses are performed for each ground motion record and totally 3000 analyses are performed for selected earthquakes within the study.

The maximum mass normalized earthquake input energies of elastic SDOF systems ($(E_I/m)_{\max}$ in m^2/s^2) are shown in Fig. 6. The graph is constituted by the maximum elastic input

Table 2 Selected earthquake ground motions (Set II: EQ 35-67) (PEER 2018)

Event Name (*2)	Station	Year	M_w	I_A (m/s)	R_{JB} (km)	V_{S30} (m/s)	PGA (g)	PGV (cm/s)	PGD (cm)
Victoria_Mexico	Victoria Hos. Sotano	1980	6.33	0	6.07	242.05	0.033	5.55	1.51
Morgan Hill	APEEL 1E – Hayward	1984	6.19	0	51.68	219.8	0.027	4.59	2.86
Morgan Hill	Agnews State Hos.	1984	6.19	0.1	24.48	239.69	0.032	5.63	2.19
Morgan Hill	Capitola	1984	6.19	0.2	39.08	288.62	0.142	8.29	1.67
Morgan Hill	Gilroy Array #2	1984	6.19	0.2	13.68	270.84	0.213	12.74	2.48
Morgan Hill	Gilroy Array #3	1984	6.19	0.3	13.01	349.85	0.201	13.30	3.66
Morgan Hill	Gilroy Array #4	1984	6.19	0.8	11.53	221.78	0.349	17.30	3.31
Morgan Hill	Gilroy Array #7	1984	6.19	0.3	12.06	333.85	0.114	5.55	1.17
Morgan Hill	Halls Valley	1984	6.19	0.9	3.45	281.61	0.312	39.32	7.02
Morgan Hill	Hollister City Hall	1984	6.19	0.2	30.76	198.77	0.071	9.91	5.27
Morgan Hill	Hollister Diff. Array #3	1984	6.19	0.1	26.42	215.54	0.079	7.05	1.41
Morgan Hill	Los Banos	1984	6.19	0	63.16	262.05	0.062	9.16	2.27
Morgan Hill	SF Intern. Airport	1984	6.19	0	70.93	190.14	0.048	2.91	0.50
Morgan Hill	San Juan B._ 24 Polk St	1984	6.19	0	27.15	335.5	0.036	4.70	1.81
Chalf. Vall.-02	Bishop–LADWP South	1986	6.19	0.5	14.38	303.47	0.176	19.53	7.09
Chalf. Vall.-02	McGee Creek - Surface	1986	6.19	0.1	28.2	359.23	0.084	2.33	0.10
Chalf. Vall.-02	Zack Brothers Ranch	1986	6.19	2	6.44	316.19	0.401	44.72	8.57
Supers. Hills-02	Brawley Airport	1987	6.54	0.3	17.03	208.71	0.111	15.99	6.90
Supers. Hills-02	Calipatria Fire Station	1987	6.54	0.5	27	205.78	0.259	14.97	3.35
Supers. Hills-02	El Centro Imp.Co.Cent	1987	6.54	1.1	18.2	192.05	0.259	41.78	21.85
Supers. Hills-02	Plaster City	1987	6.54	0.6	22.25	316.64	0.200	21.59	5.09
Supers. Hills-02	Poe Road (temp)	1987	6.54	2.1	11.16	316.64	0.286	29.01	11.36
Supers. Hills-02	Salton Sea Wildlife R.	1987	6.54	0.4	25.88	191.14	0.140	18.11	4.31
Supers. Hills-02	Westmorland Fire Sta	1987	6.54	1.2	13.03	193.67	0.211	32.32	22.31
Landers	Anaheim – W Ball Rd	1992	7.28	0.1	144.9	269.29	0.038	12.47	8.99
Landers	Arcadia – Arcadia Av	1992	7.28	0	137.25	330.5	0.028	9.24	6.62
Landers	Baker Fire Station	1992	7.28	0.3	87.94	324.62	0.106	10.97	7.96
Landers	Bell Gardens–Jaboneria	1992	7.28	0.1	154.26	267.13	0.045	13.20	16.96
Landers	Boron Fire Station	1992	7.28	0.2	89.69	291.03	0.090	9.55	3.39
Landers	Brea - S Flower Av	1992	7.28	0.1	137.44	322.75	0.044	15.10	11.91
Landers	Buena Park – La Palma	1992	7.28	0.1	150.09	270.96	0.043	13.29	19.76
Landers	Burbank – N B. Vista	1992	7.28	0.2	157.94	320.57	0.065	13.41	7.97
Landers	Compton – Castl. St	1992	7.28	0.2	161.23	266.9	0.066	13.22	11.82

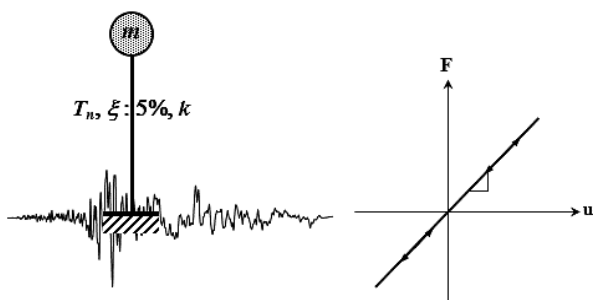


Fig. 5 Linear elastic single-degree-of-freedom (SDOF) system having $\xi=5\%$

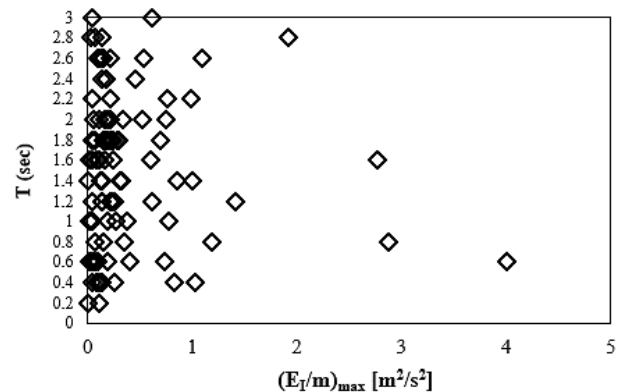


Fig. 6 The maximum mass normalized earthquake input energy values of the selected ground motion records

energies versus vibration periods of SDOF systems. The elastic input energies are obtained from the right-hand side of energy balance equality (Eq. (3)) and the maximum values of mass normalized input energies depend on the time integral of ground acceleration values multiplied by the velocity time history. The maximum mass normalized elastic input energy value is obtained from Imperial Valley-06 Earthquake (from Bonds Corner Station) within the study ($4.01 \text{ m}^2/\text{s}^2$).

The variation of the maximum mass normalized elastic input energies with Joyner-Boore (R_{JB}) distances of ground motions is presented in Fig. 7(a). The elastic input energy values generally tend to decrease with the increase in Joyner-Boore distances. The variation of the maximum

Table 3 Selected earthquake ground motions (Set III: EQ 68-100) (PEER 2018)

Event Name (*3)	Station	Year	M_w	I_A (m/s)	R_{JB} (km)	V_{S30} (m/s)	PGA (g)	PGV (cm/s)	PGD (cm)
Landers	Coolwater	1992	7.28	2.2	19.74	352.98	0.417	434.06	1524.82
Landers	Covina – W Badillo	1992	7.28	0.1	128.06	324.79	0.046	10.62	6.40
Landers	Desert Hot Springs	1992	7.28	0.7	21.78	359	0.154	20.87	7.77
Landers	Downey – Co Maint B.	1992	7.28	0.1	157.46	271.9	0.039	11.30	10.17
Landers	El Monte – Fair. Av	1992	7.28	0.1	135.88	290.63	0.038	11.81	16.12
Landers	Fountain Vall. – Euclid	1992	7.28	0.2	146.89	270.54	0.062	11.02	8.83
Landers	Hacienda Heights – C.	1992	7.28	0.1	136.29	337	0.049	8.44	4.71
Landers	Hemet Fire Station	1992	7.28	0.3	68.66	328.09	0.097	5.64	2.27
Landers	Huntington B.–Waikiki	1992	7.28	0.1	156	270.54	0.062	16.64	14.44
Landers	Indio – Coach. Canal	1992	7.28	0.3	54.25	339.02	0.109	15.11	9.79
Landers	Inglewood – Union Oil	1992	7.28	0.1	167.27	316.02	0.034	10.47	10.19
Landers	LA – 116th St School	1992	7.28	0.1	164.36	301	0.042	12.04	13.49
Landers	LA – E Vernon Ave	1992	7.28	0.1	157.69	283.14	0.041	16.20	16.34
Landers	LA – Fletcher Dr	1992	7.28	0.1	153.04	329.06	0.033	4.33	2.81
Landers	LA – N Westmoreland	1992	7.28	0.1	159.13	315.06	0.035	4.68	3.29
Landers	LA – Obregon Park	1992	7.28	0.1	151.7	349.43	0.065	7.66	5.59
Landers	LA – S Grand Ave	1992	7.28	0	161.56	285.28	0.047	17.07	21.09
Landers	LA – W 15th St	1992	7.28	0.1	160.99	329.52	0.038	12.63	15.04
Landers	LA – W 70th St	1992	7.28	0.1	163.96	241.41	0.051	14.76	12.84
Landers	LB – Orange Ave	1992	7.28	0.2	160.85	344.72	0.058	15.66	20.57
Landers	La Habra – Briarcliff	1992	7.28	0.1	143.12	338.27	0.047	11.52	8.94
Landers	La Puente – Rimg. Av	1992	7.28	0.1	132.08	339.52	0.043	9.83	4.90
Landers	Lakewood – Del A. B.	1992	7.28	0.2	157.41	267.35	0.051	15.50	14.67
Landers	Mission Creek Fault	1992	7.28	0.4	26.96	355.42	0.132	14.62	11.42
Landers	North Palm Springs	1992	7.28	0.7	26.84	344.67	0.134	14.53	5.70
Landers	Northridge–17645 Sat.	1992	7.28	0.1	172.32	280.86	0.040	16.72	16.46
Landers	Palm Springs Airport	1992	7.28	0.4	36.15	312.47	0.089	13.91	5.26
Landers	San Bern. – E & Hosp.	1992	7.28	0.4	79.76	296.97	0.087	14.57	7.63
Landers	Santa Fe Spr. – E.Joslin	1992	7.28	0.1	150.1	339.06	0.050	14.24	17.39
Landers	Sun Valley – Ros. B.	1992	7.28	0.1	163.54	320.93	0.028	8.41	5.20
Landers	Tarzana – Cedar Hill	1992	7.28	0.1	175.65	257.21	0.043	5.32	2.76
Parkfield-02, CA	Hollister–City Hall A.	2004	6.0	0	117.92	272.8	0.011	3.21	1.42
Parkfield-02, CA	Coalinga–Fire St. 39	2004	6.0	0.1	22.45	333.61	0.045	5.87	1.26

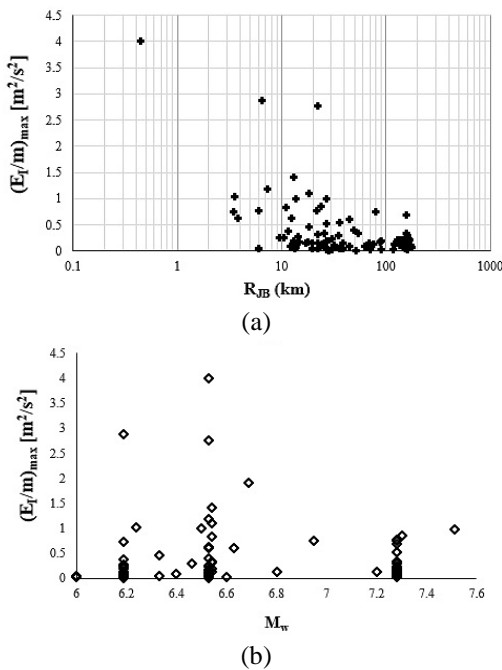


Fig. 7 Variation of the maximum mass normalized elastic input energy (a) with Joyner-Boore (R_{JB}) distance, (b) with moment magnitude (M_w) of earthquakes

mass normalized elastic input energies with moment magnitudes of selected earthquakes can be seen from Fig. 7(b). In Fig. 8(a), the relation between $(E_I/m)_{max}$ and PGA values is graphically shown for selected earthquake ground motions. The maximum mass normalized elastic input energy value is obtained from Imperial Valley-06 Earthquake (Bonds Corner Station) whose PGA value is 0.777 g (Fig. 8(a)). The values of R_{JB} , M_w , PGA and PGV for the earthquake ground motion (Imperial Valley-06/Bonds Corner Station) are given in Table 4. The variation of the maximum mass normalized elastic input energies with PGV values of earthquakes is given in Fig. 8(b). It can be seen from the graph that the values of elastic input energy generally decrease with the decrease in PGV values.

The variation of $(E_I/m)_{max}$ and R_{JB} according to the number of selected 100 earthquake ground motions is shown in Fig. 9(a). The axis of abscissa shows the number of earthquakes in Table 1, Table 2 and Table 3 and the axis of ordinate shows the maximum mass normalized elastic input energies ($(E_I/m)_{max}$) and Joyner-Boore distances (R_{JB}) according to earthquake numbers. Fig. 9(b) gives the variation of $(E_I/m)_{max}$ and M_w according to the number of selected earthquakes in Table 1, Table 2 and Table 3. In the figure, the axis of ordinate shows the maximum mass normalized elastic input energies

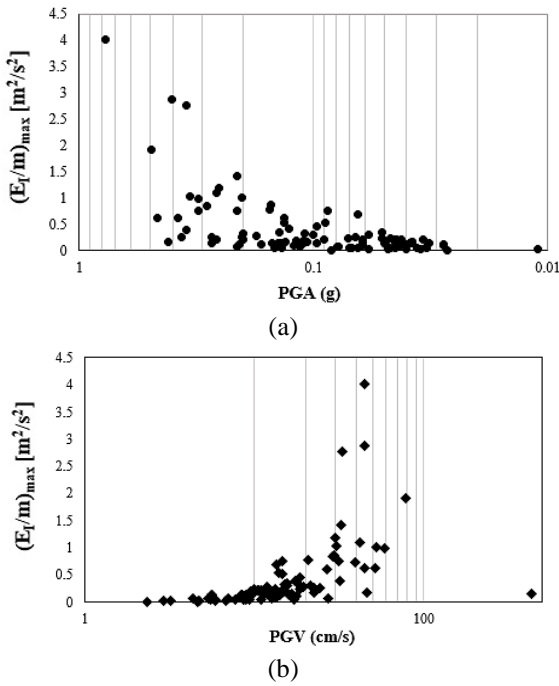


Fig. 8 Variation of the maximum mass normalized elastic input energy (a) with PGA (g), (b) with PGV (cm/s)

Table 4 R_{JB} , M_w , PGA and PGV characteristics of the ground motion which gives the maximum elastic input energy

	R_{JB} (km)	M_w	PGA (g)	PGV (cm/s)
For the Maximum $(E_I/m)_{max}$	0.44	6.53	0.777	44.93

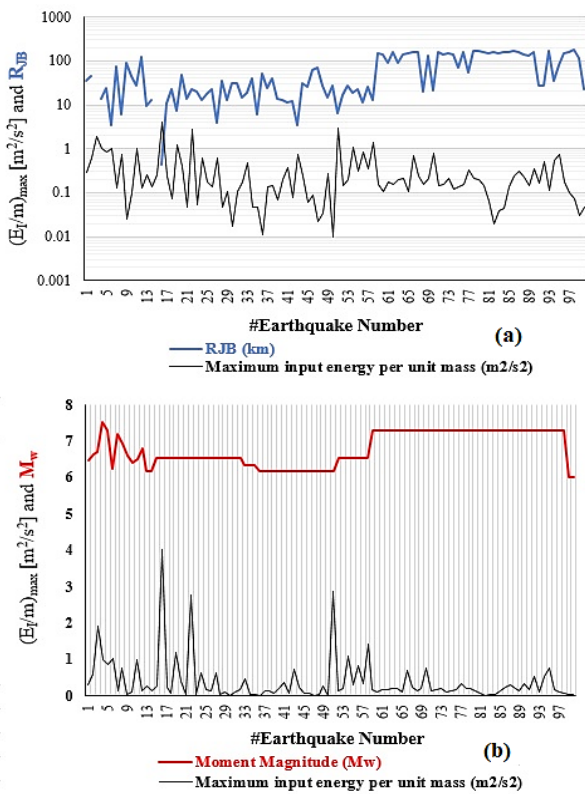


Fig. 9 The variation of (a) $(E_I/m)_{max}$ and R_{JB} , (b) $(E_I/m)_{max}$ and M_w according to the number of selected earthquakes

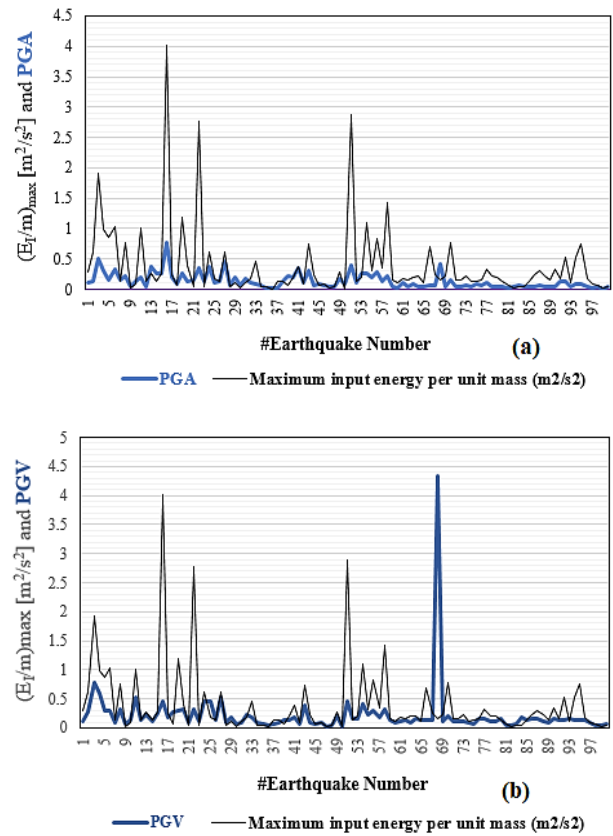


Fig. 10 The variation of (a) $(E_I/m)_{max}$ and PGA (g), (b) $(E_I/m)_{max}$ and PGV (m/s) according to the number of selected earthquakes

$(E_I/m)_{max}$ and moment magnitudes (M_w) according to earthquake numbers.

The variation of $(E_I/m)_{max}$ and PGA of selected earthquakes is shown in the same graph in Fig. 10(a). The axis of abscissa shows the number of earthquakes in Table 1, Table 2 and Table 3, as in Fig. 9. The maximum elastic input energy is obtained within the study for the earthquake whose PGA is the maximum (Imperial Valley-06 Earthquake from Bonds Corner Station). $(E_I/m)_{max}$ and PGV values are presented by the same graph of Fig. 10(b). $(E_I/m)_{max}$ and PGV values can be obtained from Fig. 10(b) according to the earthquake number. PGV values of earthquakes are indicated by the unit of m/s. It can be seen from the study that the maximum elastic input energy is not obtained for the earthquake ground motion whose PGV is the maximum.

5. Maximum elastic input energy versus pseudo-velocity relations

The maximum earthquake input energies of linear elastic SDOF systems are computed using the Excel program written by the author ($\xi=5\%$). Velocity time histories and maximum pseudo-velocities for selected earthquake records are extracted from the PRISM (2011) Earthquake Engineering Software.

Fig. 11 shows the maximum mass normalized earthquake input energy versus the maximum pseudo-velocity $((E_I/m)_{max}-S_{Vmax})$ graph (results of time history analysis). It is

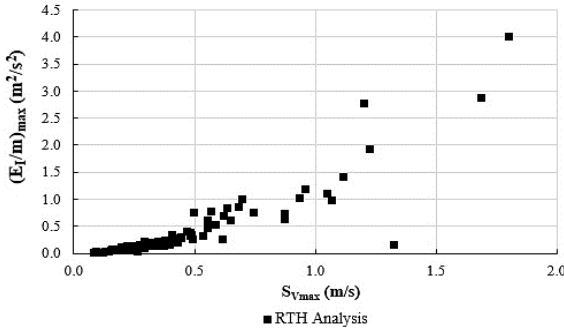


Fig. 11 The maximum mass normalized earthquake input energy versus the maximum pseudo-velocity ($(E_I/m)_{max}$ - S_{Vmax}) graph (Results of time history analysis)

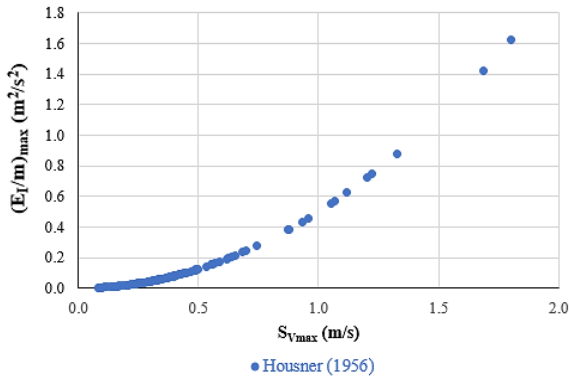


Fig. 12 The maximum mass normalized earthquake input energy versus the maximum pseudo-velocity ($(E_I/m)_{max}$ - S_{Vmax}) graph (Housner's approximation)

obviously seen that there is a proportional relation between the maximum input energy ($(E_I/m)_{max}$) and the maximum pseudo-velocity (S_{Vmax}). Housner (1956) computed firstly the input energy per unit mass of a SDOF system as follows

$$\frac{E_I}{m} = \frac{1}{2} \cdot (PSV)^2 \tag{6}$$

where m is mass of the structure and PSV is the pseudo-spectral velocity. $(E_I/m)_{max}$ - S_{Vmax} graph is regenerated for linear elastic SDOF system using Housner's approximation in Eq. (6). The relation is shown in Fig. 12.

Khashae (2004) proposed the expression for estimating seismic input energy (per unit mass) as

$$\frac{E_I}{m} = \bar{f} \cdot f_T \cdot \frac{1}{2} \cdot \left(\frac{S_a}{\omega}\right)^2 \tag{7}$$

where \bar{f} is the factor of accounting for the ductility and ground motion characteristics, f_T is the factor of period, S_a is the pseudo-acceleration and S_a/ω denotes the pseudo-spectral velocity. Khashae (2004) proposed expressions for factors of \bar{f} and f_T , using regression analysis of 160 earthquake ground motions as (Mezgebo 2015)

$$\begin{aligned} f_T &= 0.572e^{(-4.283T_n)} + 0.6 & \text{for } \mu = 1 \\ f_T &= 1 & \text{for } \mu = 2, 3, 4, 5 \\ \bar{f} &= \frac{4.256}{\sqrt{\mu - 0.5}} + 0.318I_C \end{aligned} \tag{8}$$

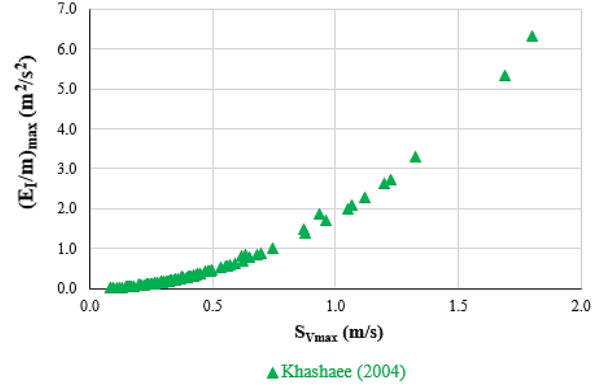


Fig. 13 The maximum mass normalized earthquake input energy versus the maximum pseudo-velocity ($(E_I/m)_{max}$ - S_{Vmax}) graph (Khashae's approximation)

where T_n is the natural period, μ is the ductility and I_C is the intensity index proposed by Park and Ang (1985), (Eq. (9)).

$$I_C = (a_{rms})^{1.5} (t_{di})^{0.5} \tag{9}$$

In Eq. (9), a_{rms} is the root-mean-square ground acceleration and t_{di} is the duration of the ground motion (Trifunac and Brady 1975). $(E_I/m)_{max}$ - S_{Vmax} graph is reobtained using Khashae's Eq. (7). f_T is calculated considering $\mu=1$ (for linear-elastic system) in Eq. (8). Fig. 13 shows the maximum mass normalized earthquake input energy versus the maximum pseudo-velocity of SDOF system (from Khashae's equation for seismic input energy).

In literature, there are many proposed equations for calculation of input energies of SDOF systems. Akiyama (1985), Kuwamura and Galambos (1989), Fajfar et. al. (1989), Uang and Bertero (1990) and Manfredi (2001) are some of the researchers who proposed input energy equations for elastic and inelastic SDOF systems. In this study, the energy results of time history analyses are compared to the results of previous researchers' approaches. Housner (1956) and Khashae's (2004) approximations are used as indicated in Eq. (6) and Eq. (7).

The input energy results are combined in a graph in Fig. 14. The figure is formed according to the earthquake number. The graph shows that Khashae's (2004) approach generally gives the maximum $(E_I/m)_{max}$ results with the proposed equation in the study (Eq. (11)).

6. Development of maximum elastic input energy equality for SDOF systems

The maximum input energy of elastic SDOF system is proposed within the study by considering the Arias Intensity and the maximum pseudo-velocity of the earthquake. Arias Intensity, as defined by Arias (1970), is proportional to the square of the ground acceleration integrated over time. Arias Intensity may be written as

$$I_A = \frac{\pi}{2g} \cdot \int_0^{t_d} a^2(t) dt \tag{10}$$

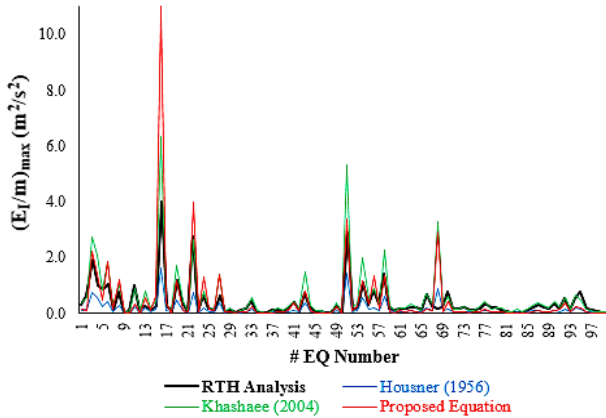


Fig. 14 The maximum mass normalized earthquake input energy values according to earthquake number (Results of ‘RTH Analysis, Housner’s (1956) equation, Khashaee’s (2004) equation, and proposed approach’), ($\zeta = 5\%$)

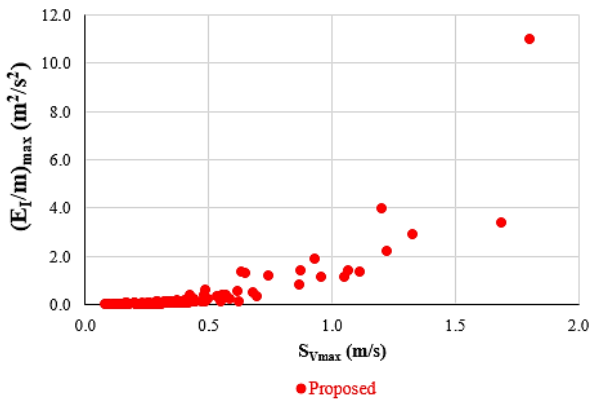


Fig. 15 The maximum mass normalized earthquake input energy versus the maximum pseudo-velocity $((E_I/m)_{max}-S_{Vmax})$ graph (proposed equation)

where $a(t)$ is the strong ground acceleration, t_d is the total earthquake duration, g is the acceleration of gravity and I_A is the Arias Intensity in m/s unit.

The maximum mass normalized earthquake input energy is formulated for selected earthquake ground motions within the study. The proposed formulation can be expressed as

$$\left(\frac{E_I}{m}\right)_{max} = S_{V_{max}} \cdot I_A \quad (11)$$

where $S_{V_{max}}$ is the maximum pseudo-spectral velocity and I_A is the Arias Intensity. Eq. (11) estimates the maximum elastic input energy per unit mass for earthquake ground motions having smaller values of Arias Intensity. In the study, the proposed formula correctly estimates the maximum mass normalized elastic input energies except for the earthquake having the largest value of Arias Intensity (Imperial Valley-06 Earthquake from Bonds Corner Station).

The maximum mass normalized earthquake input energy versus the maximum pseudo-velocity $((E_I/m)_{max}-S_{V_{max}})$ graph from the proposed equation within the study (Eq. (11)) is given in Fig. 15. It can be clearly seen from the graph that only the Imperial Valley-06 Earthquake (from

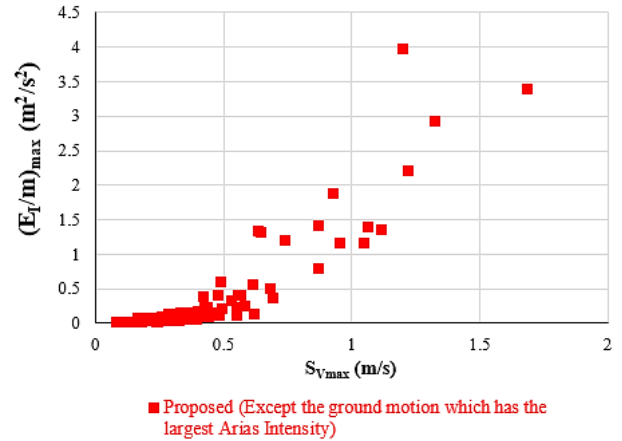


Fig. 16 The maximum mass normalized earthquake input energy versus the maximum pseudo-velocity $((E_I/m)_{max}-S_{Vmax})$ graph (proposed equation / except the ground motion having the largest I_A)

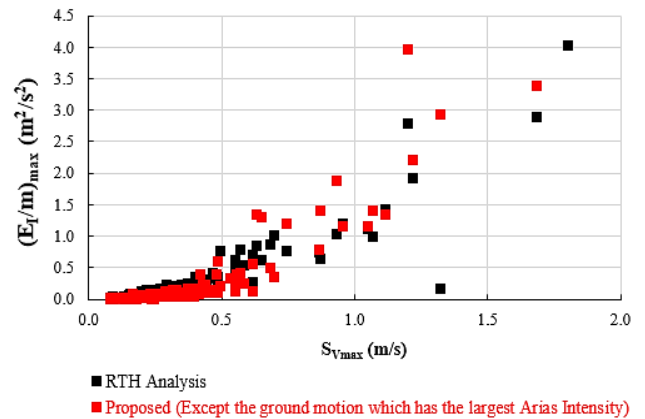


Fig. 17 The maximum mass normalized earthquake input energy versus the maximum pseudo-velocity $((E_I/m)_{max}-S_{Vmax})$ graph (Results of RTH analysis and the proposed approach)

Bonds Corner Station) gives excess input energy value. This is because the Arias Intensity value of the earthquake is the largest in selected earthquake ground motion set ($I_A=6.1$ m/s).

In Fig. 16, the maximum mass normalized earthquake input energy versus the maximum pseudo-velocity $((E_I/m)_{max}-S_{Vmax})$ graph is given with the exception of the ground motion which has the largest Arias Intensity. The results show that there is a good agreement between the maximum input energy demands of RTH (response time history) analysis and the proposed approach within the study (by Eq. (11)) (if the earthquake having the largest Arias Intensity is not taken into consideration). Fig. 17 shows the graph of the maximum mass normalized earthquake input energy versus the maximum pseudo-velocity considering time history analyses and the proposed approach. The proposed approach gives very consistent input energy results when it is compared to the results of time history analyses.

Fig. 18 and Fig. 19 shows comparative results of the maximum earthquake input energy versus the maximum pseudo-velocity. Fig. 18 compares the results of Housner’s

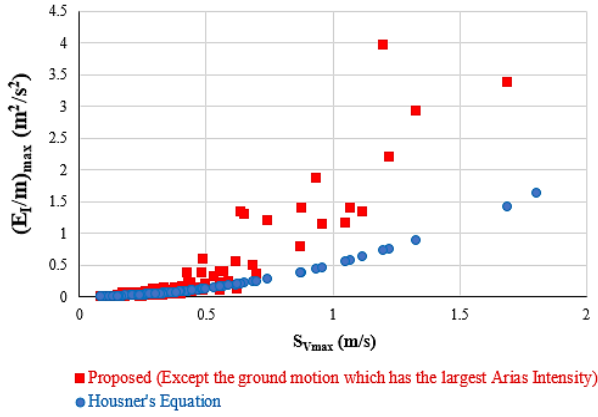


Fig. 18 The maximum mass normalized earthquake input energy versus the maximum pseudo-velocity $((E_I/m)_{max}-S_{Vmax})$ graph (Results of Housner's Equation and the proposed approach)

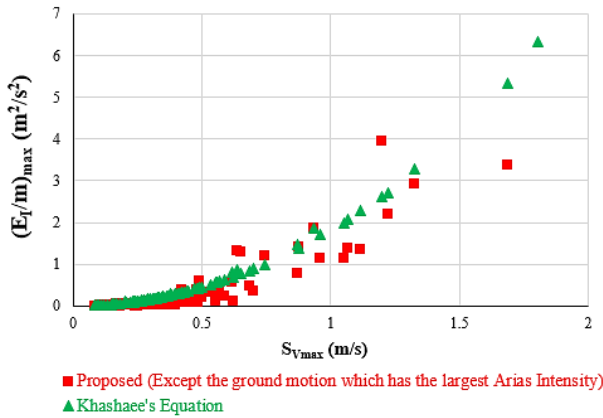


Fig. 19 The maximum mass normalized earthquake input energy versus the maximum pseudo-velocity $((E_I/m)_{max}-S_{Vmax})$ graph (Results of Khashaee's Equation and the proposed approach)

Equation and the proposed approach whereas Fig. 19 compares the results of Khashaee's Equation and the proposed approach.

The ground motion which has the largest Arias Intensity does not include in the maximum input energy results of the proposed approach. Housner's Equation and the proposed approach fits better to each other for smaller pseudo-velocity values. However, it can be directly seen from Fig. 19 that Khashaee's Equation fits much better to the proposed approach for all pseudo-velocities.

Fig. 20 and Fig. 21 show the best fitted curve for "the maximum input energy-the maximum pseudo-velocity" relation. In Fig. 20, the curve is obtained for response time history analyses and the coefficient of determination is calculated as $R^2=0.8363$. In Fig. 21, the curve is obtained for the proposed approach within the study and the coefficient of determination is calculated as $R^2=0.8442$. In the graphs, "x" defines the maximum pseudo-velocities (S_{Vmax}) and the ordinate "y" defines the maximum input energy per unit mass $((E_I/m)_{max})$.

$$(E_I / m)_{max} = 0.8874 \cdot (S_{Vmax})^2 + 0.3053 \cdot (S_{Vmax}) - 0.0144 \quad (12)$$

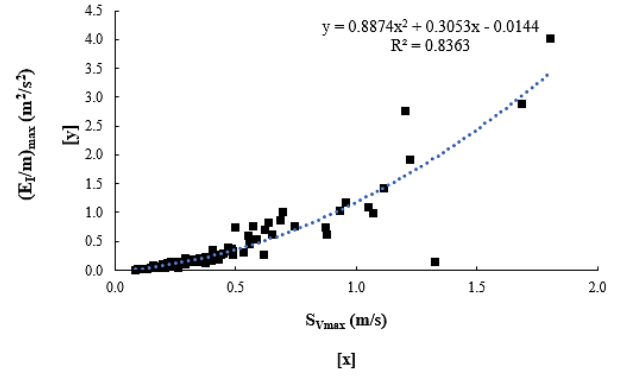


Fig. 20 Curve fitting for "the maximum input energy – the maximum pseudo-velocity" relation obtained from response time history analyses

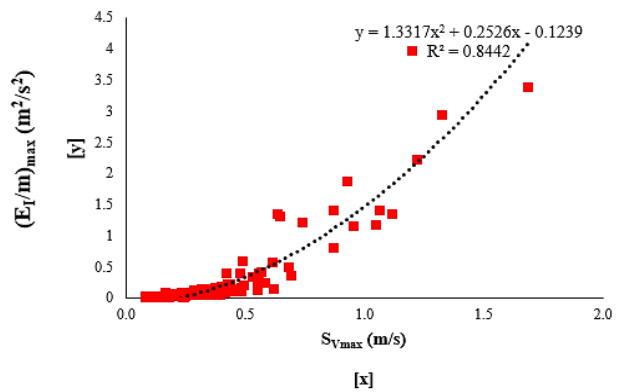


Fig. 21 Curve fitting for "the maximum input energy – the maximum pseudo-velocity" relation obtained from the proposed approach

$$(E_I / m)_{max} = 1.3317 \cdot (S_{Vmax})^2 + 0.2526 \cdot (S_{Vmax}) - 0.1239 \quad (13)$$

Eq. (12) and Eq. (13) show the equation of regression analysis and these are quadratic curves to calculate the value of $(E_I/m)_{max}$. Although the maximum earthquake input energy does not only depend on the maximum pseudo-velocity (S_{Vmax}) value, the relationship between two quantities is investigated and the maximum input energy is formulated in terms of the maximum pseudo-velocity. S_{Vmax} is in [m/s] unit and $(E_I/m)_{max}$ is in $[m^2/s^2]$ unit in Eq. (12) and Eq. (13). Determination coefficients are obtained nearly the same for the relation of " $(E_I/m)_{max}-S_{Vmax}$ " obtained both from response time history analyses and the proposed approach (Fig. 20 and Fig. 21).

It can be concluded that the proposed approach to determine the maximum input energy of an elastic SDOF system having the damping ratio of 5% is valid for earthquake ground motions which do not have larger Arias Intensity values. The proposed approach within the study correctly estimates the maximum input energy of a SDOF system for earthquake ground motions having Arias Intensity up to $I_A=3.3$ m/s.

In Fig. 22, the maximum mass normalized earthquake input energies of elastic SDOF system having damping ratio of 5% are given according to numbered earthquakes (Table 1,

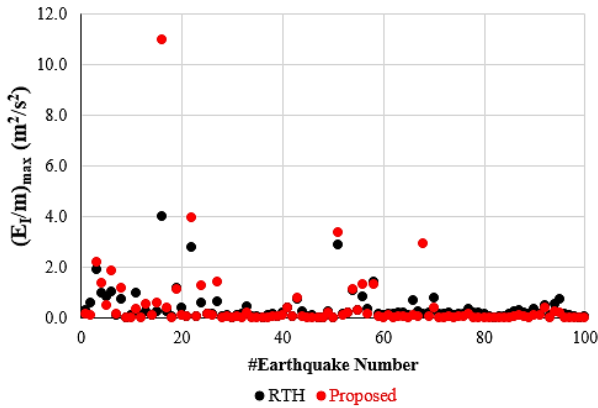


Fig. 22 $(E_f/m)_{\max}$ values in $[m^2/s^2]$ according to the number of selected earthquakes (Results of response time history analysis and the proposed approach)

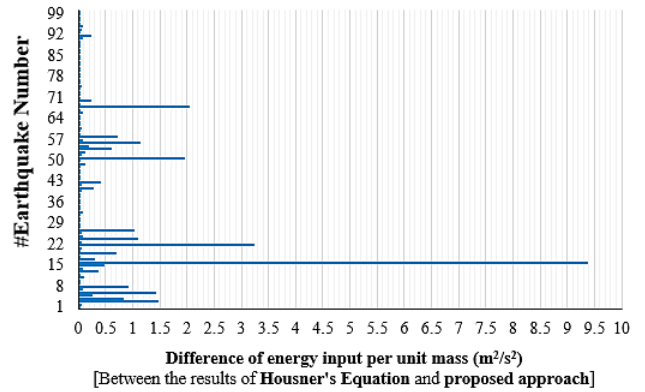


Fig. 24 Differences of energy input per unit mass [in m^2/s^2] between the results of Housner's Equation and proposed approach

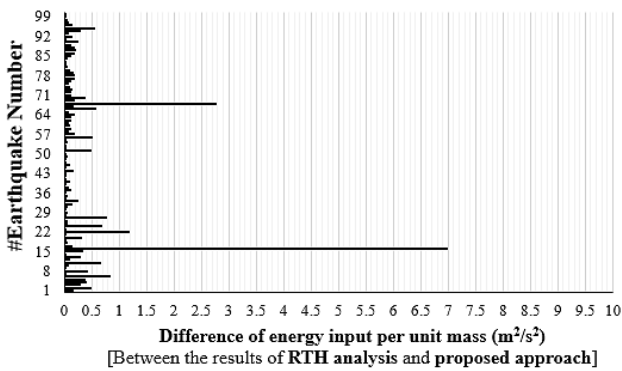


Fig. 23 Differences of energy input per unit mass [in m^2/s^2] between the results of RTH analysis and proposed approach

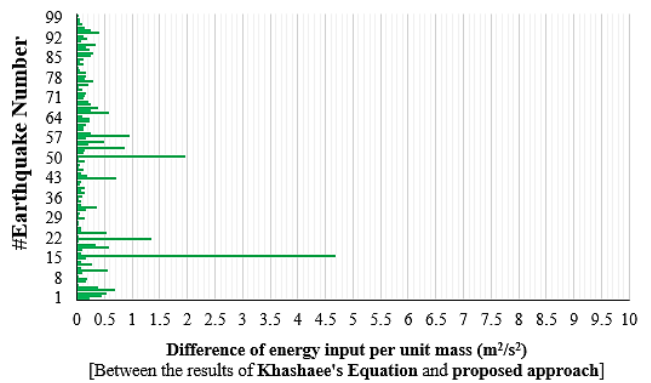


Fig. 25 Differences of energy input per unit mass [in m^2/s^2] between the results of Khashae's Equation and proposed approach

Table 2 and Table 3). The energy input results of time history analyses show good agreement with the proposed approach within the study. However, as it is expected, only the earthquake ground motion having the largest Arias Intensity in selected ground motion set (the Imperial Valley-06 Earthquake from Bonds Corner Station) gives distant result.

6.1 Differences of elastic input energy between the proposed approach and the other methods

Differences of energy input per unit mass for the proposed approach are computed and the results are presented by graphs. The results of the proposed approach are compared with the results of time history analyses and Housner's and Khashae's equations.

Input energy differences between time history analysis and the results of proposed approach are given in unit of m^2/s^2 in Fig. 23. For earthquake ground motions having larger Arias Intensity values, it can be seen that the difference between time history analysis and the proposed approach is greater. However, in general, the differences between time history analyses and the proposed approach are very small (Fig. 23).

Input energy differences between the results of Housner's Equation (Eq. (6)) and proposed approach (Eq. (11)) can be seen from Fig. 24. Fig. 25 shows the input energy differences between the results of Khashae's Equation (Eq. (7)) and proposed approach (Eq. (11)). For earthquake ground motions

having larger Arias Intensity values, it can be seen from the graphs that the differences between the proposed approach and the other approaches are greater.

Khashae's Equation for estimating seismic input energy gives the closest results with the proposed approach within the study (Fig. 19). As it is for Khashae's Equation, it can be obviously seen that the dynamic time history analyses give consistent energy results with the proposed approach, too.

It should not be forgotten that the proposed approach for computing seismic input energy is given for elastic SDOF systems having damping ratio of 5% and the results of the proposed approach can be valid under these circumstances. In this study, the time history results are used as the base because of dynamic analyses have more accurate results on computing seismic demands. To make more comparisons within the study, the proposed approach for estimating seismic input energy is compared with the results of Housner's and Khashae's Equations, too. The energy input results of proposed approach within the study can be compared with other researchers' equations to obtain more comparisons about the seismic input energy, too.

7. Conclusions

The maximum earthquake input energy is a relatively

stable response parameter to be used for energy-based seismic design of structures. It is of great importance to calculate the maximum earthquake input energy practically. To this purpose, a data set containing 100 real ground motion records which have the same soil sites has been selected within the study and response time history analyses have been performed for elastic SDOF systems having damping ratio of 5%. The maximum elastic earthquake input energy per unit mass has been computed for selected ground motion records. The computed maximum input energies from time history analyses have been given graphically according to the maximum pseudo-spectral velocities.

Previous researchers' approaches have been used to compute the maximum elastic earthquake input energy. Housner's and Khashae's Equations have been applied to SDOF systems which are under the effect of selected earthquakes. The maximum mass normalized earthquake input energy versus the maximum pseudo-velocity graphs have been obtained.

An approach which considers the pseudo-spectral velocity with Arias Intensity has been proposed to obtain the maximum elastic earthquake input energy. The maximum mass normalized earthquake input energy has been formulated for selected earthquake ground motions. The maximum elastic earthquake input energy versus the maximum pseudo-velocity graphs have also been obtained using the proposed approach. Quadratic curves have been fitted to compute the maximum elastic earthquake input energy according to the maximum pseudo-velocity. The maximum input energy values of time history analyses and Housner's and Khashae's Equations have been compared to the maximum input energy values of the proposed approach.

The results of the study are restricted to the selected ground motions which are on the soil site with $180 \text{ m/s} < V_{S30} \leq 360 \text{ m/s}$. The notable findings of the study are as follows:

- A good agreement is achieved between the maximum input energy demands of response time history analysis and the other approaches (including the proposed approach).
- The proposed formula within the study correctly estimates the maximum mass normalized elastic input energies for ground motions that do not have larger Arias Intensity values.
- The proposed approach for estimating the maximum elastic earthquake input energy shows great agreement with Khashae's approach.
- It is observed from the study that the maximum elastic earthquake input energy of near fault earthquakes are higher than that of the far fault records.
- When the maximum elastic earthquake input energy versus the maximum pseudo-velocity graph is obtained using the proposed approach, it has been observed that the input energy varies with the square of the maximum pseudo-velocity. This point can be obviously seen from Housner's and Khashae's approaches, too.
- The input energy results show that each earthquake reflects its own characteristics in dynamic analyses and in seismic energy computations.

Further studies can be done using wide range of ground motion records which are on different soil sites. Different

approaches of other scientists can be considered too in order to compare the maximum elastic input energy of the proposed approach. The study can be extended for multi-degree-of-freedom (MDOF) systems and for systems having different damping ratios. The maximum earthquake input energy of inelastic systems which have different ductility ratios can be investigated, too.

References

- Akbas, B. (1997), "Energy-based earthquake resistant design of steel moment resisting frames", Ph.D. Dissertation, Graduate College of Illinois Institute of Technology, Illinois.
- Akbas, B. and Shen, J. (2003), "Earthquake-resistant design (EQRD) and energy concepts", *Tech. J.*, **192**, 2877-2901. (in Turkish)
- Akbas, B., Shen, J. and Hao, H. (2001), "Energy approach in performance-based seismic design of steel moment resisting frames for basic safety objective", *Struct. Des. Tall Build.*, **10**(3), 193-217.
- Akbas, B., Shen, J. and Temiz, H. (2006), "Identifying the hysteretic energy demand and distribution in regular steel frames", *Steel Compos. Struct.*, **6**(6), 479-491.
- Akbas, B., Tugsal, U.M. and Kara, F.I. (2009), "An evaluation of energy response and cumulative plastic rotation demand in steel moment resisting frames through dynamic/static pushover analyses", *Struct. Des. Tall Spec. Build.*, **18**(4), 405-426.
- Akiyama, H. (1985), *Earthquake-Resistant Limit-State Design for Buildings*, University of Tokyo Press, Tokyo, Japan.
- Arias, A. (1970), *A Measure of Earthquake Intensity in Seismic Design for Nuclear Power Plants*, The MIT Press, Cambridge, Massachusetts.
- ASCE (2010), Minimum Design Loads for Buildings and Other Structures, ASCE/SEI Standard 7-10; USA.
- ATC (1996), Seismic Evaluation and Retrofit of Concrete Buildings, ATC-40: Applied Technology Council, Redwood City, CA, USA.
- Benavent-Climent, A., Pujades, L.G. and López-Almansa, F. (2002), "Design energy input spectra for moderate seismicity regions", *Earthq. Eng. Struct. Dyn.*, **31**, 1151-1172.
- Bojórquez, E., Teran-Gilmore, A., Ruiz, S.E. and Reyes-Salazar, A. (2011), "Evaluation of structural reliability of steel frames: Interstory drift versus plastic hysteretic energy", *Earthq. Spectra*, **27**(3), 661-682.
- BSSC (2009), National Earthquake Hazards Reduction Program Recommended Seismic Provisions for New Buildings and Other Structures, Part 1: Provisions, Building Seismic Safety Council, Federal Emergency Management Agency (FEMA P-750), Washington, D.C.
- Canadian Commission on Building and Fire Code (1995), National Building Code of Canada, National Research Council of Canada, Ottawa, Ontario.
- CEN (2004), Eurocode 8: Design of Structures for Earthquake Resistance - Part 1: General Rules, Seismic Actions and Rules for Buildings, European Committee for Standardization, Brussels, Belgium.
- Chopra, A.K. (1995), *Dynamics of Structures, Theory and Applications to Earthquake Engineering*, Prentice Hall, Upper Saddle River, N.J.
- Decanini, L.D. and Mollaioli, F. (1998), "Formulation of elastic earthquake input energy spectra", *Earthq. Eng. Struct. Dyn.*, **27**, 1503-1522.
- Dindar, A.A., Yalcin, C., Yuksel, E., Ozkaynak, H. and Buyukozturk, O. (2015), "Development of earthquake energy demand spectra", *Earthq. Spectra*, **31**(3), 1667-1689.

- Enderami, S.A., Beheshti-Aval, S.B. and Saadeghvaziri, M.A. (2014), "New energy-based approach to predict seismic demands of steel moment resisting frames subjected to near-fault ground motions", *Eng. Struct.*, **72**, 182-192.
- Fajfar, P. and Fischinger, M.A. (1990), "Seismic procedure including energy concept", *Ninth European Conference on Earthquake Engineering (ECEE)*, Moscow.
- Fajfar, P. and Vidic, T., (1994), "Consistent inelastic design spectra: hysteretic and input energy", *Earthq. Eng. Struct. Dyn.*, **23**, 523-537.
- Fajfar, P., Vidic, T. and Fischinger, M. (1989), "Seismic demand in medium- and long-period structures", *Earthq. Eng. Struct. Dyn.*, **18**(8), 1133-1144.
- FEMA 440 (2005), Improvement of Nonlinear Static Seismic Analysis Procedures, Federal Emergency Management Agency, Washington, D.C.
- Gullu, A., Yuksel, E. and Yalcin, C. (2018), "Seismic energy based design: numerical evaluation of diverse MDOF systems", *Proceedings of the 16th European Conference on Earthquake Engineering*, Thessaloniki.
- Gullu, A., Yuksel, E., Yalcin, C., Dindar, A.A. and Ozkaynak, H. (2017), "Experimental verification of the elastic input energy spectrum and a suggestion", *Proceedings of the Interdisciplinary Perspectives for Future Building Envelopes*, Istanbul, Turkey, May.
- Housner, G.W. (1956), "Limit design of structures to resist earthquakes", *Proceedings of the 1st World Conference on Earthquake Engineering*, Oakland, California, USA.
- IBC 2006 (2006), International Building Code, International Code Council, Country Club Hills, Illinois, USA.
- Khashae, P. (2004), "Energy-based seismic design and damage assessment for structures", Ph.D. Dissertation, Southern Methodist University, Dallas, Texas.
- Kuwamura, H. and Galambos, T.V. (1989), "Earthquake load for structural reliability", *J. Struct. Eng.*, **115**(6), 1446-1462.
- Lee, S.S. and Goel, S.C. (2001), "Performance based design of steel moment frames using target drift and yield mechanism", Research Report (UMCEE 01-17), The University of Michigan, Department of Civil and Environmental Engineering.
- Leelataviwat, S., Goel, S.C. and Stojadinovic, B. (2002), "Energy-based seismic design of structures using yield mechanism and target drift", *J. Struct. Eng.*, **128**(8), 1046-1054.
- Liao, W.C. (2010), "Performance-based plastic design of earthquake resistant reinforced concrete moment frames", Ph.D. Dissertation, University of Michigan, Ann Arbor, USA.
- López-Almansa, F., Yazgan, A.U. and Benavent-Climent, A. (2013), "Design energy input spectra for high seismicity regions based on Turkish registers", *Bull. Earthq. Eng.*, **11**(4), 885-912.
- Manfredi, G. (2001), "Evaluation of seismic energy demand", *Earthq. Eng. Struct. Dyn.*, **30**(4), 485-499.
- Merter, O. and Ucar, T. (2017), "Energy-based design base shear for RC frames considering global failure mechanism and reduced hysteretic behavior", *Struct. Eng. Mech.*, **63**(1), 23-35.
- Mezgebo, M. and Lui, E.M. (2016), "Hysteresis and soil site dependent input and hysteretic energy spectra for far-source ground motions", *Adv. Civil Eng.*, **2016**, 1-29.
- Mezgebo, M.G. (2015), "Estimation of earthquake input energy, hysteretic energy and its distribution in MDOF structures", Ph.D. Dissertation, Syracuse University, New York.
- Ozсарac, V., Karimzadeh, S., Erberik, M.A. and Askan, A. (2017), "Energy-based response of simple structural systems by using simulated ground motions", *Procedia Eng.*, **199**, 236-241.
- Park, Y. and Ang, A. (1985), "Mechanistic seismic damage model for reinforced concrete", *J. Struct. Eng.*, **111**(4), 722-739.
- PEER (2018), Pacific Earthquake Engineering Research Center Strong Ground Motion Database, <http://ngawest2.berkeley.edu/>.
- PRISM for Earthquake Engineering (2011), A Software for Seismic Response Analysis of Single-Degree-of Freedom Systems, Department of Architectural Engineering, INHA University.
- Riddell, R. and Garcia, J.E. (2001), "Hysteretic energy spectrum and damage control", *Earthq. Eng. Struct. Dyn.*, **30**, 1791-1816.
- Taflampas, I.M., Maniatakis, C.A. and Spyarakos, C.C. (2008), "Estimation of input seismic energy by means of a new definition of strong motion duration", *The 14th World Conference on Earthquake Engineering*, Beijing, China.
- TBEC (2018), Turkish Building Earthquake Code, The Disaster and Emergency Management Presidency of Turkey, 18th of March of Official Gazette, Ankara, Turkey.
- Trifunac, M.D. and Brady, A.G. (1975), "A Study on the duration of strong earthquake ground motion", *Bull. Seismol. Soc. Am.*, **65**, 581-626.
- TSDC (2007), Turkish Seismic Design Code, Ministry of Public Works and Settlement, Ankara, Turkey
- Uang, C.M. and Bertero, V.V. (1990), "Evaluation of seismic energy in structures", *Earthq. Eng. Struct. Dyn.*, **19**(1), 77-90.
- UBC (1997), Uniform Building Code, International Conference of Building Officials, Whittier, California, USA.
- Ucar, T., Merter, O. and Duzgun, M. (2012), "A study on determination of target displacement of RC frames using PSV spectrum and energy-balance concept", *Struct. Eng. Mech.*, **41**(6), 759-773.
- Zahrah, T.F. and Hall, W.J. (1984), "Earthquake energy absorption in SDOF Structures", *J. Struct. Eng.*, **110**, 1757-1773.

CC